CrystEngComm

PAPER

View Article Online
View Journal | View Issue

CrossMark click for updates

Cite this: *CrystEngComm*, 2016, **18**, 616

Synthesis of Cu/ZnO core/shell nanocomposites and their use as efficient photocatalysts

Shu-Hao Chang, Po-Yuan Yang, Chien-Ming Lai, Shu-Chen Lu, Guo-An Li, Wei-Chung Chang and Hsing-Yu Tuan*

Received 2nd October 2015,
Accepted 17th December 2015

DOI: 10.1039/c5ce01944c

www.rsc.org/crystengcomm

The synthesis of a metal/semiconductor (Cu/ZnO) core/shell nanostructure consisting of Cu nanoparticles with an average diameter of 44.4 ± 4.3 nm and coated with a 4.8 ± 0.5 nm-thick layer of ZnO is reported. The Cu/ZnO core/shell nanomaterials were formed by rapidly injecting a mixture of copper(I) chloride, zinc acetate and oleylamine (OLA) solution into a hot OLA solution at 320 °C for 5 min. Both the Cu (core) and ZnO (shell) parts were crystalline according to X-ray diffraction, selected area electron diffraction (SAED), and high-resolution transmission electron microscopy (HRTEM) analyses. The Cu/ZnO core/shell nanomaterials acted as an efficient photocalyst and degraded the pollutant methylene blue, whereas pure Cu nanoparticles did not. The average degradation rate constant of methylene blue by the Cu/ZnO heterostructures was determined to be 1.708 h^{-1}, much higher than those of commercial ZnO (1.628 h^{-1}) and TiO_2 (0.307 h^{-1}), showing that the Cu/ZnO core/shell heterostructure is a promising photocatalyst for pollutant degradation.

Introduction

Surface-modified nanosized cores with inorganic shells, so-called core/shell nanomaterials, constitute a type of heterostructure normally containing two or more nanometer-sized components in an onion-like hybrid structure that are prepared in a controlled way. These heterostructures can usually display improved properties and provide multiple functions that may not be provided by the corresponding single-component nanomaterials.[1] These hybrid structures have shown special physical and chemical properties and have become the most promising candidates for new fields in optical,[2–5] electrical[6,7] and biomedical[8–10] applications. As the demand for various core/shell nanomaterials and nanostructures has increased, it is becoming critical to develop new approaches for fabricating a wide variety of core/shell nanomaterials in order to modify or improve the properties of single-component nanomaterials. Coating a thin shell, such as silica coating, on the various nanomaterials not only assists in providing multiple functions but also provides surface passivation.[11,12] For example, recent developments in chemical synthesis have allowed the controllable preparation of different species of core/shell metal-semiconductor heterostructures, such as Ag/ZnO,[13,14] Ag/TiO_2 (ref. 15) and Au/TiO_2.[16] In comparison to pure semiconductors, some core/shell structures, such as CdS/TiO_2,[17,18] ZnO/ZnSe (ref. 19, 20) and SnO_2/CdS,[21] have shown higher photocatalytic efficiency.

Zinc oxide (ZnO) is a well-studied environmentally friendly nanomaterial potentially suitable for energy industry applications due to its transparency and good semiconductor characteristics, in particular its wide band gap (3.37 eV at room temperature) with an exciton binding energy of 60 meV.[22] Its features yield a strong near-band-edge excitonic emission at a wide range of temperatures.[22,23] ZnO has been widely used as a transparent oxide semiconductor that possesses piezoelectric properties.[22] The unique optical and catalytic properties of ZnO nanostructures have attracted much attention for photovoltaics,[24,25] photosensors[26,27] and light-emitting diodes (LED).[28,29] ZnO has been especially considered as a good photocatalytic material due to its UV and visible optical absorption and photoluminescence. On the other hand, copper is a well-known material in our daily life, and is highly conductive, making it suitable for applications in printed circuit boards (PCBs)[29] at a comparatively low cost. Furthermore, Cu nanomaterials exhibit localized surface plasmon resonance (LSPR)[30] when electromagnetic radiation excites the free electrons of the metallic nanostructure, which results in oscillations that enhance the local electromagnetic fields surrounding the nanostructure.[30] The frequency and the line width of the LSPR are highly affected by the morphology, interparticle spacing, dielectric environment, and dielectric properties of the nanomaterial.[31–33] Therefore, an appropriate strategy for preparing Cu/ZnO nanocomposites can effect efficient charge separation *via* direct electron transfer of hot

Department of Chemical Engineering, National Tsing Hua University, 101, Section 2, Kuang-Fu Road, Hsinchu, Taiwan 30013, Republic of China.
E-mail: hytuan@che.nthu.edu.tw; Fax: +886 3 571 5408; Tel: +886 3 572 3661

electrons induced by surface plasmon resonance from Cu, and thus achieve good photocatalytic efficiency.

Herein, a facile method to prepare a multifunctional Cu/ZnO core/shell structure is reported. Cu nanoparticles with an average diameter of 44.4 ± 4.3 nm and covered with a 4.8 ± 0.5 nm-thick ZnO layer were prepared by rapidly injecting a mixture of copper(I) chloride, zinc acetate and oleylamine (OLA) solution into a hot OLA solution at 280–320 °C. With precise control of the experimental conditions, a ZnO shell directly grew onto the copper nanoparticles. The products were characterized by transmission electron microscopy (TEM), X-ray diffraction (XRD) and UV-vis absorbance spectrophotometry. The use of these Cu/ZnO core/shell colloids as a photocatalyst to degrade methylene blue was also demonstrated.

Experimental

Chemicals

All reagents were used as received. Copper(I) chloride (CuCl, ≧99.99%), zinc acetate ($Zn(CH_3COO)_2$, ≧99.99%), mercaptopropionic acid (MPA, ≧99%), ammonia solution (NH_4OH, 33%), hexane, toluene, chloroform, oleylamine (70%), ethanol, methylene blue (≧99%), titanium(IV) oxide (P25-nano grade), and ZnO powders were obtained from Aldrich Chemical. Methanol was obtained from Mallinckrodt Chemicals, and isopropyl alcohol from J. T. Baker.

Cu/ZnO core/shell nanomaterial synthesis

Reactions were carried out using a Schlenk line system under a purified argon atmosphere. In the typical synthesis, 8 ml oleylamine and a stir bar were loaded into a 50 mL three-neck flask. The flask was purged by argon for 1 h at room temperature and the temperature was then raised to 320 °C. Copper(I) chloride (1 mmol) and zinc acetate (1 mmol) were mixed with 1 mL oleylamine and heated to 100 °C. Copper and zinc precursor solutions were injected into the flask and kept at a temperature of 300 °C for 5 min. The flask was cooled to room temperature by using a cold water bath. The nanocrystals were purified by precipitation with addition of 20 mL of toluene followed by centrifugation at 8000 rpm for 5 min. The isolated nanomaterials were dispersed in toluene for further characterization.

Surface modification of Cu/ZnO core/shell nanomaterial

Two millilitres of chloroform, 5 mL of methanol, 180 μL MPA and 280 μL ammonia solution were mixed with the Cu/ZnO powder and stirred vigorously for 30 min. After the reaction, 5 mL of isopropyl alcohol and 20 mL of hexane were added followed by centrifugation at 8000 rpm for 10 min. After purification, the product was redispersed in DI water for further characterization.

Photocatalytic activity measurements

Photocatalytic activities of the different samples were evaluated by the degradation of methylene blue under UV irradiation. A UV lamp (256 nm) was used to generate light for the photocatalytic reaction, which was carried out under the reaction cell. All of the experiments were conducted at room temperature and were open to the atmosphere. In each experiment, 20 mg of Cu/ZnO core/shell nanomaterials were added into 20 mL of methylene blue solution in a reaction cell. At irradiation time intervals of 0, 5, 10, 30, 60, 90, and 120 min, the suspension was collected by applying centrifugation (8000 rpm, 5 min) to remove the photocatalyst nanomaterials, which were characterized using UV-vis absorbance spectroscopy.

Characterization

Nanomaterials were characterized by using various techniques, including transmission electron microscopy (TEM), X-ray diffraction (XRD) and UV-vis absorbance spectroscopy. The sample for TEM was prepared by dropping the nanocrystals dispersed in hexane or DI water on carbon-coated 200 mesh titanium or nickel TEM grids. TEM images were obtained using a JEOL JEM-1200 or Hitachi H-7100 TEM at an accelerating voltage of 120 kV for low-resolution imaging and using a Tecnai G2 F20 X-Twin microscope at an accelerating voltage of 200 kV for high-resolution imaging. Powder X-ray diffraction (XRD) analysis was conducted on a Rigaku Ultima IV X-ray diffractometer using a Cu Kα radiation source (λ = 1.54 Å). UV-vis-NIR absorbance spectra of nanocrystal dispersions in DI were obtained by using a Hitachi U-4100 UV-vis-NIR spectrophotometer at room temperature.

Results and discussion

The core/shell structure of Cu/ZnO was produced using a hot-injection approach in the presence of oleylamine. Copper chloride and zinc acetate served as precursors and oleylamine was chosen as the surfactant for the high-temperature reaction. The degassed oleylamine was heated to 320 °C followed by the injection of copper chloride and zinc acetate dissolved in the oleylamine. When many copper nuclei were generated, the concentration of the precursor decreased and the nuclei began to grow followed by formation of zinc oxide. ZnO nucleated on the surface of the Cu nanoparticles and grew to become a thin ZnO layer during the synthesis. The XRD pattern of the product was compared with and interpreted based upon a standard database. The characteristic copper peaks appeared at 43.3° and 50.4°, which correspond to the (111) and (200) crystal facets of copper. The three main characteristic peaks for ZnO appeared in the sample at 31.8°, 34.4° and 36.3°, which correspond to the (100), (002) and (101) crystal facets of ZnO. These results confirmed that two different groups of peaks corresponding to copper and zinc oxide could be clearly distinguished in the XRD pattern (Fig. 1).

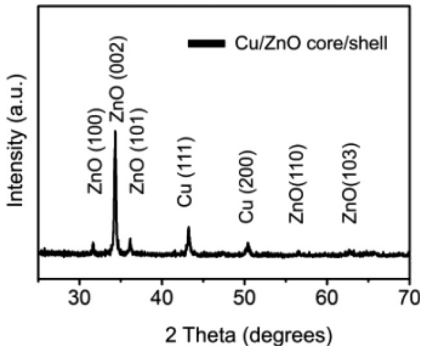

Fig. 1 XRD pattern of Cu/ZnO core/shell nanomaterials.

The morphology and composition of the products were examined by TEM and EDS (Fig. 2). TEM images confirmed that a thin layer of material existed on the core of nanoparticles. The core had a mean diameter of 44.4 ± 4.3 nm and was covered with a 4.8 ± 0.5 nm-thick shell. We analyzed the selected area electron diffraction (SAED) pattern and the fringe distance corresponding to copper and zinc oxide, respectively. The formation of ZnO along with the copper nanoparticles in the hot-injection process can be attributed to the sudden nucleation of zinc oxide on the core. Core/shell nanoparticles were randomly chosen for TEM energy-dispersive X-ray spectroscopy (EDS) analysis, and the atomic compositions determined from EDS were Cu : Zn : O = 46.7 : 27.7 : 25.6. The result showed that the sample contained Cu, Zn and O with the Zn/O ratio close to 1. Core/shell heterostructures, which are formed by the growth of crystalline overlayers onto the nanocrystal surface, enable the passivation of interfaces and have been used to generate several devices with diverse functions. Normally, the compatibility of the lattice constants of the two materials affects their ability to form a heterointerface. It is easier to form heterostructures when the component crystal structures are compatible and the lattice spacings of the two materials are well matched. However, in some special cases, dehydrolysis may help form a heterostructure despite a large lattice mismatch, such as for Ag/ZnO. In the incompatible Cu/ZnO system, the absence of a surfactant may induce the formation of the core/shell.

Fig. 3 shows the high-resolution transmission electron microscopy (HRTEM) image of a representative Cu/ZnO core/shell nanoparticle. The 0.18 nm and 0.24 nm lattice fringes correspond to the Cu (200) and ZnO (101) lattice fringes, respectively. The Cu/ZnO heterostructures accommodated the large mismatch with a value of 33.3%. The large lattice mismatch between the Cu core and the ZnO shell creates a barrier for nucleation of the shell material. The defects and dislocations inside the shell cause a highly strained interface inside the nanocrystal and poor control over the kinetics of shell growth.

Fig. 4 shows typical UV-vis optical absorption spectra of the Cu/ZnO core/shell heterostructure. Two obvious peaks in this spectrum, at 374 nm and 586 nm, were generated by zinc oxide and copper-containing materials, respectively. From the spectrum, the band gap of ZnO was estimated to be 3.3 eV. As the size of the ZnO shell is larger than its Bohr radius of 2.3 nm, the blue shift of the UV spectrum was not clearly observed.

The reaction temperatures were maintained at the desired temperature range from 280 °C to 320 °C. The same reaction was carried out at different temperatures by the hot-injection method in OLA. At 280 °C, some purely ZnO nanoparticles formed, and did not nucleate and grow on the surfaces of the copper nanocrystals. The Cu nanoparticles displayed a wide distribution of sizes. Relatively small Cu nanoparticles of 24.7 ± 9.6 nm in diameter were obtained at 280 °C (Fig. 5a) and larger nanoparticles of 56.4 ± 7.0 nm in diameter were prepared at 320 °C (Fig. 5c).

Methylene blue, a chemically stable and persistent dye pollutant, is widely adopted as a representative organic pollutant.[34] Here we evaluated the photocatalytic performance of the Cu/ZnO heterostructure nanocatalyst by monitoring its decomposition of methylene blue in an aqueous solution. In order to explore the photocatalytic efficiency of the nanocatalysts in the aqueous phase, it was essential to carry out a hydrophilic to hydrophobic ligand exchange reaction. The effective ligand exchange of a long-alkane-chain surfactant

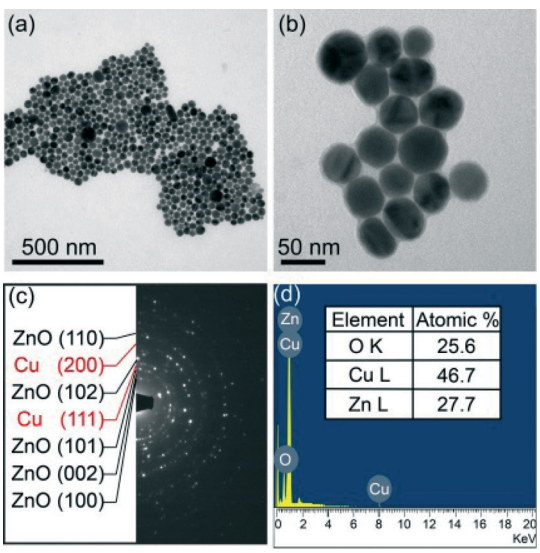

Fig. 2 (a, b) TEM image, (c) SAED pattern and (d) EDS spectrum of Cu/ZnO core/shell nanomaterials.

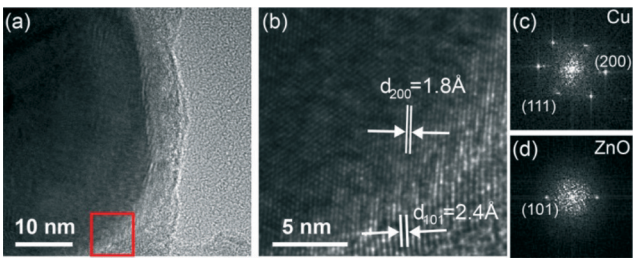

Fig. 3 (a) TEM, (b) HRTEM, and (c, d) corresponding FFT patterns of Cu/ZnO core/shell heterostructures.

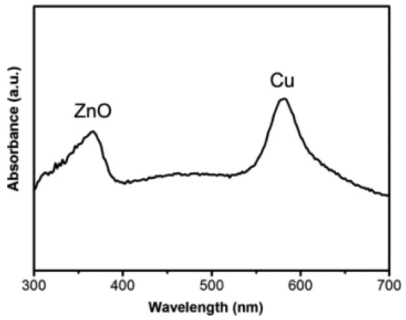

Fig. 4 UV-vis absorbance spectrum of a Cu/ZnO core/shell nanomaterial.

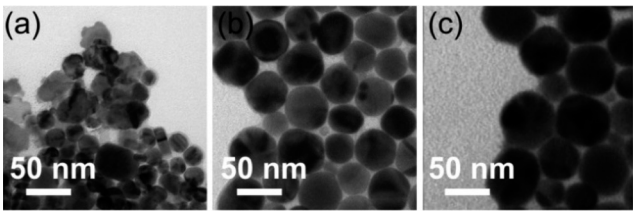

Fig. 5 TEM images of Cu/ZnO prepared at reaction temperatures of (a) 280 °C, (b) 300 °C and (c) 320 °C.

(oleylamine) by a short-chain surfactant (MPA) drastically changed the surface properties of Cu/ZnO heterostructure nanomaterials, which allowed these nanomaterials to undergo the photocatalytic reaction in aqueous solution. The XRD and UV-vis patterns of the product of the ligand exchange process were compared to the reactant. They shared the same crystal phase according to the XRD data. The UV-vis absorbance spectra also showed the two characteristic peaks to be at the same position (Fig. 6). In the experiments, the commercial TiO_2 (P-25) and ZnO powder (1 μm) were used as a reference to understand the photocatalytic activity of the Cu/ZnO catalysts. The band gap of ZnO derived from the UV-vis spectrum confers on the nanomaterials the ability to absorb UV light for photocatalytic decomposition of methylene blue. Fig. 7 shows the photocatalytic activities of pure Cu, Cu/ZnO heterostructures and TiO_2 (P25), and commercial ZnO on the degradation of methylene blue. Under the same experimental conditions, the visible-light ($\lambda > 420$ nm) photolysis of methylene blue was negligible for each of the photocatalysts. After 2 h of UV-light irradiation, degradation of the

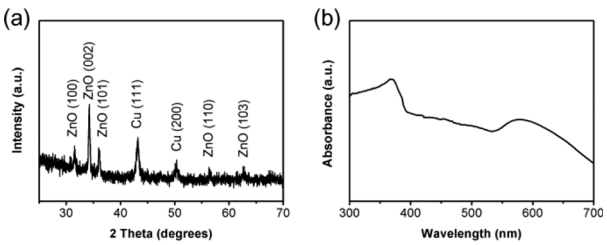

Fig. 6 (a) XRD pattern and (b) UV-vis absorbance spectra of Cu/ZnO heterostructure nanomaterials after the ligand exchange process.

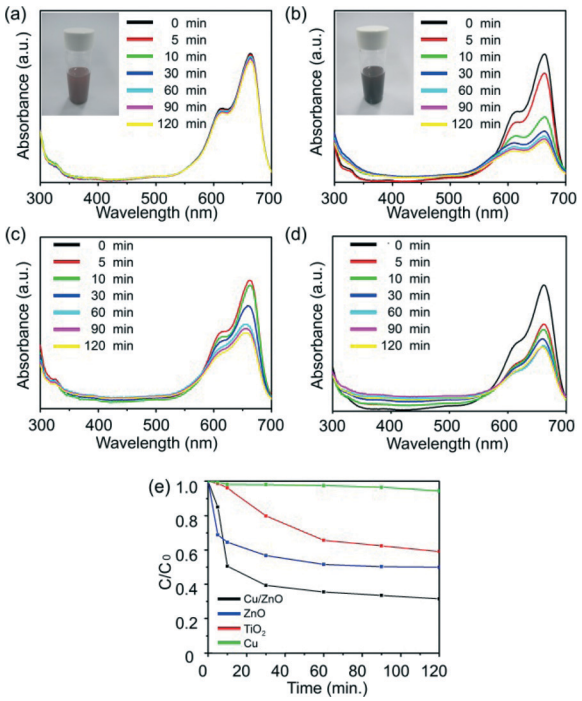

Fig. 7 Photocatalytic activity of (a) Cu, (b) Cu/ZnO, (c) TiO_2, and (d) ZnO as photocatalysts for degradation of methylene blue in the aqueous phase. (e) Comparison of the photocatalytic efficiency values of the four different materials.

dye was not detected when using pure Cu. In contrast, the Cu/ZnO heterostructures showed an excellent level of methylene blue photodegradation, even better than did the commercial TiO_2 and ZnO. The percentage of degradation of methylene blue is reported as C/C_0. C is the concentration derived from the absorption spectra of methylene blue for each irradiated time interval at a wavelength of 256 nm. C_0 is the absorption of the starting concentration when adsorption/desorption equilibrium was achieved. To quantitatively analyse the reaction kinetics of the methylene blue degradation in our experiments, we used the pseudo-first-order model as expressed by eqn (1), which is suitable if the initial concentration of the pollutant is low (36).

$$\ln(C_0/C) = kt \quad (1)$$

In eqn (1), C_0 and C are the concentrations of dye in solution at time 0 and t, respectively, and k is the pseudo-first-order rate constant.

The methylene blue average degradation rate constant when using Cu/ZnO heterostructures reached 1.708 h^{-1}, higher than those when using ZnO (1.628 h^{-1}), TiO_2 (0.307 h^{-1}) and Cu (0.048 h^{-1}). These results suggest that the Cu/ZnO heterostructure is a much more effective photocatalyst and suggest that the Cu/ZnO heterojunction thus enhances photocatalytic activity significantly.

A possible reason for these results is that Cu nanoparticles may act as the sink to receive the electrons from ZnO under excitation, which would increase the interfacial

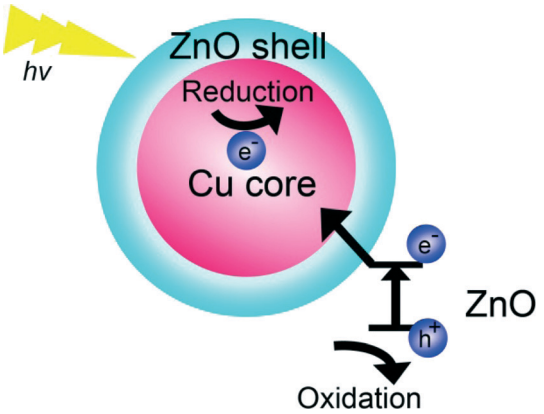

Fig. 8 Scheme of a light-induced charge separation mechanism in the Cu/ZnO heterostructure in a photocatalytic reaction.

charge-transfer kinetics between the metal core and the semiconductor shell. At the interface of two materials, the Fermi energy levels would be aligned by electrons flowing from one component to the other. In our case, the electrons would have flowed from ZnO into the Cu metal and formed a Schottky barrier resulting in the Cu having excess negative charges (electrons) and the semiconductor having excess positive charges (holes). Furthermore, the Schottky barrier would be able to prevent electron–hole recombination in the photocatalytic reaction. The unique structure would improve the separation of photogenerated electron–hole pairs, and enhance the photocatalytic activity as shown in Fig. 8.

Conclusions

A crystalline Cu/ZnO core/shell nanostructure was made by applying a hot-injection method to decompose copper(I) chloride and zinc acetate at 280–320 °C. The heterostructures exhibited outstanding performance for methylene blue degradation, better than that displayed by commercial TiO_2. The novel heterostructure represents a new hybrid material that can trigger a light-induced charge separation and that could be used for many other applications to achieve a better photon-induced catalytic efficiency.

Acknowledgements

H.-Y. T. acknowledges the financial support by the Ministry of Science and Technology through the grants of NSC 102-2221-E-007-023-MY3, MOST 103-2221-E-007-089-MY3, MOST 103-2622-E-007-025, and MOST 102-2633-M-007-002.

References

1 T. Zhou, M. Lu, Z. Zhang, H. Gong, W. S. Chin and B. Liu, *Adv. Mater.*, 2010, **22**, 403–406.
2 X. Peng, M. C. Schlamp, A. V. Kadavanich and A. Alivisatos, *J. Am. Chem. Soc.*, 1997, **119**, 7019–7029.
3 L. Kong, W. Chen, D. Ma, Y. Yang, S. Liu and S. Huang, *J. Mater. Chem.*, 2012, **22**, 719–724.
4 C. Xue, X. Chen, S. J. Hurst and C. A. Mirkin, *Adv. Mater.*, 2007, **19**, 4071–4074.
5 D. V. Talapin, I. Mekis, S. Götzinger, A. Kornowski, O. Benson and H. Weller, *J. Phys. Chem. B*, 2004, **108**, 18826–18831.
6 C.-H. Kuo, Y.-C. Yang, S. Gwo and M. H. Huang, *J. Am. Chem. Soc.*, 2011, **133**, 1052–1057.
7 J.-S. Lee, E. V. Shevchenko and D. V. Talapin, *J. Am. Chem. Soc.*, 2008, **130**, 9673–9675.
8 S.-H. Choi, H. B. Na, Y. I. Park, K. An, S. G. Kwon, Y. Jang, M.-H. Park, J. Moon, J. S. Son and I. C. Song, *J. Am. Chem. Soc.*, 2008, **130**, 15573–15580.
9 Y. Qiang, J. Antony, A. Sharma, J. Nutting, D. Sikes and D. Meyer, *J. Nanopart. Res.*, 2006, **8**, 489–496.
10 L. Zhou, J. Yuan and Y. Wei, *J. Mater. Chem.*, 2011, **21**, 2823–2840.
11 A. Guerrero-Martínez, J. Pérez-Juste and L. M. Liz-Marzán, *Adv. Mater.*, 2010, **22**, 1182–1195.
12 S.-H. Chang, Y.-T. Tsai, G.-A. Li, S.-L. Jheng, T.-L. Kao and H.-Y. Tuan, *RSC Adv.*, 2014, **4**, 40146–40151.
13 H. R. Liu, G. X. Shao, J. F. Zhao, Z. X. Zhang, Y. Zhang, J. Liang, X. G. Liu, H. S. Jia and B. S. Xu, *J. Phys. Chem. C*, 2012, **116**, 16182–16190.
14 F.-R. Fan, Y. Ding, D.-Y. Liu, Z.-Q. Tian and Z. L. Wang, *J. Am. Chem. Soc.*, 2009, **131**, 12036–12037.
15 I. Pastoriza-Santos, D. S. Koktysh, A. A. Mamedov, M. Giersig, N. A. Kotov and L. M. Liz-Marzán, *Langmuir*, 2000, **16**, 2731–2735.
16 X.-F. Wu, H.-Y. Song, J.-M. Yoon, Y.-T. Yu and Y.-F. Chen, *Langmuir*, 2009, **25**, 6438–6447.
17 S. Liu, N. Zhang, Z.-R. Tang and Y.-J. Xu, *ACS Appl. Mater. Interfaces*, 2012, **4**, 6378–6385.
18 J. Li, M. W. Hoffmann, H. Shen, C. Fabrega, J. D. Prades, T. Andreu, F. Hernandez-Ramirez and S. Mathur, *J. Mater. Chem.*, 2012, **22**, 20472–20476.
19 S. Cho, J.-W. Jang, J. Kim, J. S. Lee, W. Choi and K.-H. Lee, *Langmuir*, 2011, **27**, 10243–10250.
20 S. Cho, J.-W. Jang, J. S. Lee and K.-H. Lee, *Nanoscale*, 2012, **4**, 2066–2071.
21 A. Kar, S. Kundu and A. Patra, *RSC Adv.*, 2012, **2**, 10222–10230.
22 Ü. Özgür, Y. I. Alivov, C. Liu, A. Teke, M. Reshchikov, S. Doğan, V. Avrutin, S.-J. Cho and H. Morkoc, *J. Appl. Phys.*, 2005, **98**, 041301.
23 T. Voss, C. Bekeny, L. Wischmeier, H. Gafsi, S. Börner, W. Schade, A. Mofor, A. Bakin and A. Waag, *Appl. Phys. Lett.*, 2006, **89**, 182107.
24 M. White, D. Olson, S. Shaheen, N. Kopidakis and D. S. Ginley, *Appl. Phys. Lett.*, 2006, **89**, 143517.
25 K. S. Leschkies, R. Divakar, J. Basu, E. Enache-Pommer, J. E. Boercker, C. B. Carter, U. R. Kortshagen, D. J. Norris and E. S. Aydil, *Nano Lett.*, 2007, **7**, 1793–1798.
26 J. Suehiro, N. Nakagawa, S.-I. Hidaka, M. Ueda, K. Imasaka, M. Higashihata, T. Okada and M. Hara, *Nanotechnology*, 2006, **17**, 2567.
27 Y. K. Su, S. M. Peng, L. W. Ji, C. Z. Wu, W. B. Cheng and C. H. Liu, *Langmuir*, 2010, **26**, 603–606.
28 J.-H. Lim, C.-K. Kang, K.-K. Kim, I.-K. Park, D.-K. Hwang and S.-J. Park, *Adv. Mater.*, 2006, **18**, 2720–2724.

29 Y. Zhang, L. Ge, M. Li, M. Yan, S. Ge, J. Yu, X. Song and B. Cao, *Chem. Commun.*, 2014, **50**, 1417–1419.
30 G. H. Chan, J. Zhao, E. M. Hicks, G. C. Schatz and R. P. Van Duyne, *Nano Lett.*, 2007, **7**, 1947–1952.
31 Q. Darugar, W. Qian, M. A. El-Sayed and M.-P. Pileni, *J. Phys. Chem. B*, 2006, **110**, 143–149.
32 B. Sepúlveda, P. C. Angelomé, L. M. Lechuga and L. M. Liz-Marzán, *Nano Today*, 2009, **4**, 244–251.
33 K. A. Willets and R. P. Van Duyne, *Annu. Rev. Phys. Chem.*, 2007, **58**, 267–297.
34 L. Li, P. A. Salvador and G. S. Rohrer, *Nanoscale*, 2014, **6**, 24–42.